Engineered Science
DOI: https://dx.doi.org/10.30919/es1299

Thermal Cooling Enhancement of 18650 Cylindrical Electric Vehicle Battery Module with Mini-channel Fins Heat Sink Units Using Nanofluids Mixed Flow Channel

Sarawut Sirikasemsuk,[1] Ponthep Vengsungnle,[2] Jarinee Jongpluempiti,[2] Smith Eiamsa-ard,[3] Phumisak Tangmunpoowadol[4] and Paisarn Naphon[4,*]

Abstract

Numerical analysis and testing were conducted to predict the cooling removal ability of a pack utilizing ferrofluid flowing via a channel lined with different mini-channel heat sink units. The battery module components are made of aluminum blocks. In this study, sixty 18650 batteries are evaluated in a cylindrical form at a total voltage and current of 25.2V and 30A, respectively. This study selected improving the properties of the coolant and the flow surface area to improve the battery thermal cooling. The integrated heat sink unit has a larger surface area and more flow disruption of the coolant running through it. As a result, Models I and II exhibit the greatest and lowest temperatures, respectively. The cell maximum temperatures are 30.91 °C (Model I), 30.10 °C (Model II), 30.11 °C (Model III), and 30.12 °C (Model IV). Furthermore, Models I, II, III, and IV exhibit temperature gradients of 2.35 °C, 1.48 °C, 1.56 °C, and 1.61 °C, respectively. These findings have significant significance for the evolution of the battery thermal management system, as they explore several heat transfer enhancement approaches for improving thermal cooling to obtain safe and stable operation.

Keywords: Thermal cooling; Electric vehicle battery module; Mini-channel heat sink; Nanofluids.
Received: 26 August 2024; Revised: 20 October 2024; Accepted: 01 November 2024.
Article type: Research article.

1. Introduction

The battery temperature management systems are critical for maximizing the potential of electric vehicles. Many variables influence the decision to adopt a cooling system for thermal management, such as vehicle performance requirements, financial constraints, and present environmental conditions. The battery thermal management system (BTMS) is designed to withstand harsh designing temperatures, making it an essential component of any current electric vehicle (EV).[1] It can keep the working temperature within the limits specified range.[2]

The National Renewable Energy Laboratory (NREL) analyzed the pack's thermal performance and temperature distribution.[3] BTMS can generally be classified as air cooling, liquid cooling, phase change materials (PCM), or a combination system.[4] Each cooling technique has benefits and downsides, as seen in Fig. 1. Because of their small size and cheap cost, early-stage EV vehicles often employ passive ambient air cooling. High ambient temperatures (over 35.00 °C) considerably influence passive cooling efficiency.[5] Consequently, EVs equipped with air conditioning may only be driven in cold or mild weather.

In contrast to passive air cooling, active cooling may require storage energy, lowering overall driving efficiency. The cooling medium may significantly influence the active BTMS cooling efficacy. Air cooling is widely recognized for

[1] *Department of Mechanical Engineering, Faculty of Engineering and Architecture, Rajamangala University of Technology Suvarnabhumi, Phranakhon Si Ayutthaya, 13000, Thailand.*
[2] *Department of Agricultural Machinery Engineering, Faculty of Engineering and Architecture, Rajamangala University of Technology Isan, Nakhonratchasima, 30000, Thailand.*
[3] *Department of Mechanical Engineering, Faculty of Engineering, Mahanakorn University of Technology, Bangkok, 10530, Thailand.*
[4] *Department of Mechanical Engineering, Faculty of Engineering, Srinakharinwirot University, 63 Rangsit-Nakhornnayok Rd., Ongkharak, Nakhorn-Nayok, 26120, Thailand.*
**Email:* paisarnn@g.swu.ac.th (P. Naphon)

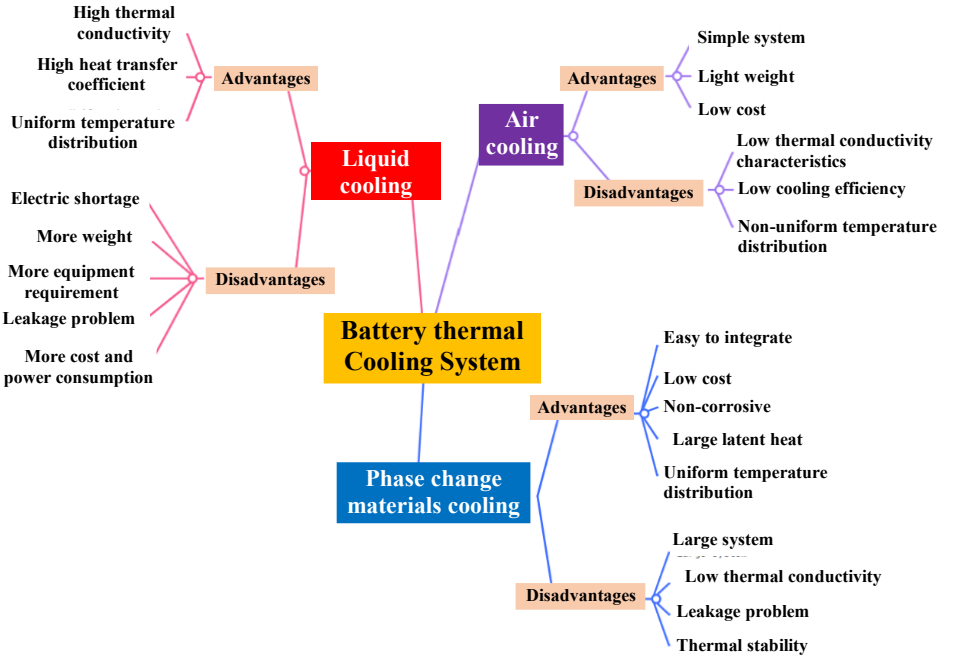

Fig. 1 Summary of each battery thermal management system's advantages and disadvantages.

its exceptional compactness, durability, and affordable production and maintenance costs.[6] However, Chen *et al*.[7] studied the fact that air cooling needed more energy than liquid cooling at the same temperature. Cooling PCM often achieves higher temperature homogeneity than other methods.[8] However, PCM is commonly regarded as a viable integrated system in other BTMSs to capitalize on its latent heat benefits.[9] A liquid cooling system provides higher thermal efficiency than an air cooling system.[10] Many experimental data indicate that liquid cooling may reduce temperature rises more effectively than PCM and air cooling.[11] This study will look at current research on liquid cooling for BTMSs to learn more about this technology's heat transfer and dissipation potentials. Liquid-cooling BTMS and vehicle powertrains rely on water/glycol solvent as the most common coolant. The freezing point of water is reduced by using ethylene glycol.[12]

The properties of the coolant have a significant effect on BTMS cooling performance. The heat removal ability of oil coolants is generally 1.5-3 times that of air. Nanoparticles may be mixed into ordinary liquid coolants to enhance thermal conductivity.[13,14] Because of their high heat conductivity and low viscosity, liquid metals such as mercury and gallium alloys might be used as coolants, but they are much more costly than water and oil.[15,16] Optimizing the liquid-cooling BTMS design and structure is crucial for enhancing overall cooling performance, as shown in Fig. 2.

1.1 Coolant channel improvement

The flow channel is a crucial component of a liquid-cooling system, transferring heat from the cells to the coolant running through it. The channel design improvements are mainly intended to improve thermal performance and low energy consumption. Zhao *et al*.[17] designed a cooling system using a mini-channel-embedded cylinder. Lan *et al*.[18] proposed a mini-channel tube for a cell that discharges at various speeds.

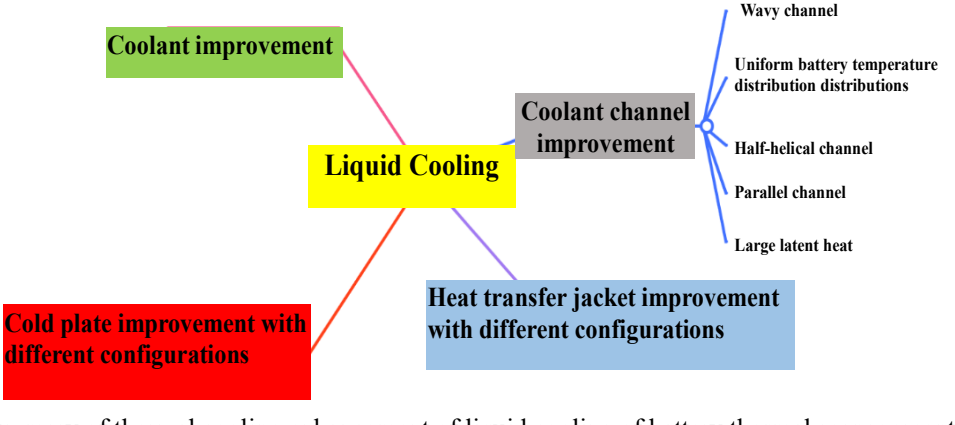

Fig. 2 Summary of thermal cooling enhancement of liquid cooling of battery thermal management system.

The optimal design keeps the temperature at its maximum of 27.80 °C, with a temperature gradient of 0.80 °C for discharge rates of 1C, 1.5C, and 2C. Jiaqiang *et al.*[19] and Cao *et al.*[20] looked into the effect of the mini-channel on thermal cooling at the battery pack system level. The optimization work involved modifying the T-junction to improve thermal cooling performance. The temperature difference of 11.00 °C is the most significant temperature during 2C discharge at 38.85 °C. Sheng *et al.*[21] created a liquid-cooling BTMS with two inlets and outputs with different locations, channel widths, and flow orientations. Xie *et al.*[22] developed a channel liquid-cooling system for the serpentine channel's inner surface. Temperature uniformity and heat transfer between battery cells and liquid coolants may be significantly improved due to the increased mixing flows in the channel caused by the redesigned baffles. Li *et al.*[23] studied the performance of a liquid-cooling system for Lithium-ion battery (LIB) cells with a discharge rate of 3C. Li *et al.*[24] developed a new wavy cooling channel liquid-cooling system. When discharged at 5C, the designed channel decreased the highest temperature and temperature gradient by 12.80 °C and 5.30 °C, respectively.

1.2 Heat transfer jacket improvement

A jacket connects the cells to the coolant flowing in the cooling system. Heat transfer efficiency has a substantial influence on system cooling performance. The jacket upgrades are often obtained by swapping conducting materials or modifying the configuration of the flow channel. Chen *et al.*[25] applied the metal shell as a spreader jacket with higher cooling performance. Coleman *et al.*[26] added aluminum and metal wax to the liquid cooling system for better heat removal. The predicted results demonstrated that the modified system offers appropriate cooling efficiency under typical conditions. Zhang *et al.*[27] employed flexible graphite plates with thermal solid conductivity for the cooling system with a reduced temperature gradient of 5.00 °C. Zhang *et al.*[28] modified the cooling jacket of a BTMS using a sodium polyacrylate hydrogel and a composite silica gel plate.[29] Rao *et al.*[30] studied a cooling jacket for the pack. The best design lowered the highest temperature and weight by 28.00% and 47.00%, respectively. Tang *et al.*[31] created and enhanced a contact surface-based area for the 18,650 lithium battery cells. Using a contact surface angle of 15° and 2C discharge resulted in outstanding cooling performance, with a temperature gradient of 2.58 °C. Li *et al.*[32] designed a novel jacket for a liquid-cooled system, reducing the highest temperature and temperature gradient.

1.3 Cold plate improvement

The liquid-cooled system uses a cooling plate made of thin metal with coolant channels circulating through it.[33] Jarrett *et al.* [34] and Smith *et al.*[35] examined three types of liquid-cooled cold plates. It was discovered that all systems give enough cooling ability for the pack. Jin *et al.*[36] improved the cooling system with embedded fins. The increased heat transport maintained the cell temperature below 50 °C. De Vita *et al.*[37] created a cold plate for cooling performance enhancement of prismatic LIB cells. Simulations proved the design capacity to keep temperature rise less than 2.50 ºC. Li *et al.*[38] employed an aluminum chamber with a grooved surface for a cold plate. Tong *et al.*[39] determined how many prismatic battery cells could be placed between two cold plates. The battery module maintains an average temperature of < 39.85 °C. Huo *et al.*[40] employed aluminum cold plates and mini-channel designs to cool lithium-ion prismatic cells. Qian *et al.*[41] tuned four essential variables of the cold system, and it was found that the highest temperature and temperature gradients were reduced by 13.30% and 43.30%, respectively. Wang *et al.*[42] developed a thermal silica cold plate to enhance the cooling mechanism in prismatic LIB cells. Wang *et al.*[43] developed a thermal silica cold plate system to maintain temperatures below 42.00 °C. Patil *et al.*[44] The cold plate was used to cool LIB pouch cells to lower the maximum temperature and temperature differential. Karthik *et al.*[45] employed a multi-objective evolutionary algorithm to optimize the coolant flow rates. Chen *et al.*[46] created an artificial neural network (ANN) with three essential criteria to predict the peak temperature and energy requirement of a cold plate system of LIB cells. A successful quick charging-cooling schedule may maintain the highest temperature below 33.35 °C. Garg *et al.*[47] used Thompson sampling's approach to improve three critically relevant parameters. Wang *et al.*[48] experimentally studied three essential cold plate parameters in a liquid-cooled system using a prismatic pack. For maximum temperature, the best combination is 28.32 °C with a 3.02 °C difference.

1.4 Coolant improvement

The primary coolant upgrade consists of changing a standard liquid coolant without substantially modifying the existing liquid-cooling system, in which the liquid-cooling systems often employ dielectric coolant. Van Gils *et al.*[49] demonstrated a dielectric coolant to consider the effect of boiling operations on thermal cooling performance. Wang *et al.*[50] also employed hydrofluoroether-7000, a nonflammable, dielectric refrigerant, as the working fluid in a cooled system. Hirano *et al.*[51] applied a cooling technique to increase the cooling thermal removal ability. Despite high cyclic charging and discharging rates, the batteries remained at a maximum

temperature of 35 °C. An *et al.*[52] introduced a cooled system with the dielectric hydrofluoroether liquid as a coolant. Tan *et al.*[53] studied a cooling system for a LIB pack with a charging rate of 3C. Al-Zareer *et al.*[54] studied the liquid cooling system using pressurized ammonia and liquid metal as a coolant.[55,56] The metal coolant has about 50 times the thermal conductivity and six times the density of water, which means that the liquid metal can keep the pack under the designed temperature. Li *et al.*[57] used a PCM solution flowing in the cooling system for the pack. The velocity and concentration of coolant significantly affect the peak temperature. The most effective investigation was by Naphon *et al.*[58-64], who continuously performed tests and numerical calculations. They examined a liquid cooling system with varying coolant kinds, flow directions, and electric car batteries. The cooling system of the pack with different nanofluids, including AgO nanofluids,[65] Al_2O_3, or CuO nanofluids.[66] Kritzer *et al.*[67] employed pressurized CO_2 as a working fluid flowing in the cooling system for battery packs in high-temperature environments, avoiding fire and thermal runaway. Chen *et al.*[68] created cooling scheduling algorithms to achieve thermal management goals. It is found that the peak temperature is less than 26 °C (0.5C), 32 °C (1C) and 40 °C (1.5C). Chang *et al.*[69] created a liquid-cooling system that uses reciprocating flow. The peak and average temperature gradient decrease by 1.67 and 3.77 °C. Recent research has examined the power capabilities of cells with varying degrees of health and compared the performance of four conventional lithium-ion batteries with phase change materials in comparable circuit models.[70-72]

The heat generated by the energy storage power pack during operation is complex, significantly influencing the thermal performance and lifetime of the energy storage. Consequently, thermal cooling is essential to keep the system working correctly. Liquid cooling performs more in heat removal ability and controlling temperature, making it a good alternative for high-performance applications. Air conditioning, on the other hand, is a straightforward and affordable feature that is appropriate for certain car types. As EV technology improves, the development of heat management systems is critical to realizing the full potential of electric mobility. Many variables influence the decision to adopt a cooling system for thermal management, such as vehicle performance requirements, financial constraints, and present environmental conditions. As previously stated, the power pack is cooled using many cooling methods. Understanding how chemical phenomena, peak temperature, and temperature fluctuate with operating circumstances is critical. The current study continuously used numerical analysis and experimentation to estimate the cylindrical Li-ion pack's temperature distribution and maximum temperature using a ferrofluid cooling system flowing through a channel lined with heat sink units. The derived results are verified with the measured data.[58-64]

2. Experimental apparatus and procedure

As shown in Fig. 3, the cylindrical lithium-ion battery unit is an experimental setup. Cooling by refrigeration, cooling by hot-side ferrofluid, cooling by cold-side refrigeration, and electrical control are the four primary loops just before it enters the hot side flow channel of the thermoelectric module, the refrigeration cooling loop chills the hot side coolant loop. The R134a refrigerator cooling system controls and chills the intake hot side coolant before it enters the thermoelectric cooling module. A peristaltic pump, a magnetic pump, and an ultrasonic bath make up the hot side ferrofluid cooling loop. With a series of steps beginning with suction from the ultrasonic bath and ending with its return to the bath, the ferrofluid travels via the flowmeter and into the hot side flow channel of the thermoelectric cooling module (TCM). The accurate receiver and stopwatch record the rate of flow. In contrast to the flowmeters, which measure the rate of coolant flow, the digital weight scale measures the mass of the fluid with a full-scale accuracy of 0.01%. A longer peristaltic pump may produce pulsing ferrofluid flows, while a water pump can carry out continuous ferrofluid flows via the thermoelectric cooling module. When it comes to monitoring the temperatures of the coolant at the intake and outlet ports of the TCM hot side, all type-T thermocouples provide an accuracy of 0.1% of full-scale reading. Connected to the computer, the Datataker DT85 records them every three seconds. The components of the cold side water loop were the storage tank, flowmeter, test section unit (battery pack), and radiator. First, the test part (the electric car battery pack) receives the pumped and supplied coolant, which lowers the temperature. After that, it returns to the tank via the heat exchanger, where it is heated and then released into the surrounding environment. We can measure the coolant temperature at different points by applying four type-T thermocouples pre-calibrated with a dry block type calibrator.

Electric automobiles and other portable electronics are only two of the many growing markets for Li-ion batteries. Researchers only needed one row of sixty cylindrical lithium-ion battery cells for this investigation. In Table 1, you can see the details of the 18650-cylinder cell. The electric vehicle's battery pack consists of a battery and a liquid cooling package, as seen in Fig. 4. The main cooling block and two cover plates made of aluminum make up the liquid cooling package. On

the left side of the main cooling block in the center zone are the 60 cylindrical holes that measure 18.44 × 65.21 mm in diameter and height. On the right side of the block are the top flow channels, and in the middle zone are the 60 holes for cylindrical battery cells. Install screws into the rubber gasket that covers the main cooling block's two side interfaces and secures them to the cover plate. Then, use the thermal insulator Aeroflex sheet to cover it and keep the heat in. The SUNKCO 709A and similar pulse spot welding machines connect the copper wires to the electric car BTMs and the nickel plate, which holds the battery cell poles. The BMS controls the voltage and current that reach the battery pack. In order to determine the distribution of temperatures, a Datataker DT85 connected to a computer takes data from each of the thermocouples. Mounted on the primary surface of the battery cells, seven type-T thermocouples make up the middle zone of the cell height. The current method for determining the coolant's temperature uses four thermocouples.

This is because the ambient air temperature affects the thermal performance of the EV battery pack. Therefore, the test room temperature is controlled at a constant ambient temperature of 25 ºC. The relevant instruments have uncertainty and accuracy, as shown in Table 2. First, in this experiment, the charged and discharged processes are performed without liquid cooling circulation for different current rates (1A, 2A, 4A) to consider the transient thermal response of the battery unit with operating time. As expected, the discharge/charge current rates significantly affect the module's overall temperature. Suppose using a very high charge/discharge current. The battery cell is whole and runs

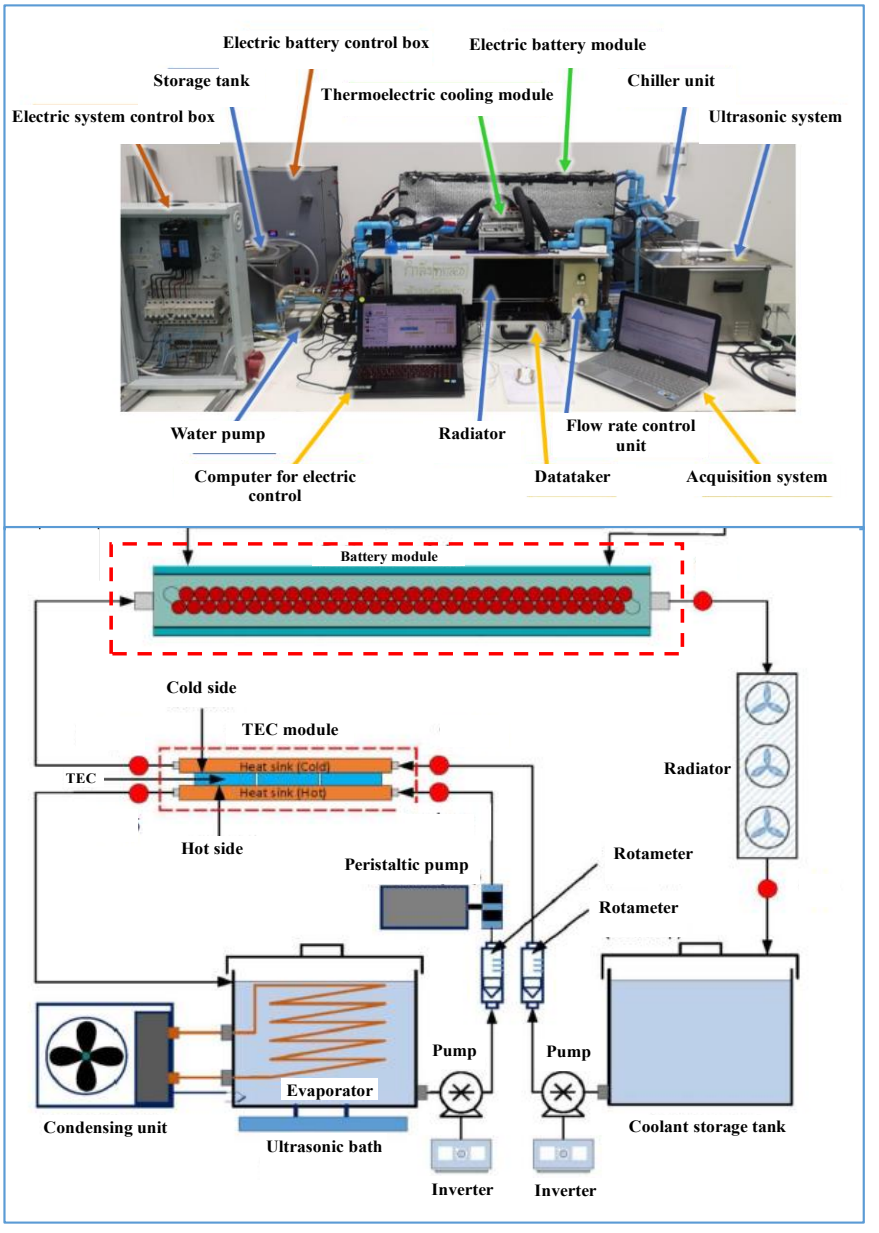

Fig. 3 Schematic diagram of the experimental apparatus.

out quickly, making it challenging to observe the changing battery temperature. Therefore, the charged and discharged processes are performed at the current 1A, 2A, and 4A rates (More details, see [59]). The most common way to charge lithium-ion batteries is using a CC-CV charger. In terms of timing, the charging of constant current devices occurs before the charging of constant voltage devices. Connecting the charger to the battery activates the CC mode, which keeps the electric current constant.

Table 1. Details of the 18650-type cylindrical battery cell.[54]

Properties	Specification
Electrolyte material chemistry	$LiMn_2O_4$
Diameter	18.43 mm
Height	65.21 mm
Weight	40.6 g
Nominal capacity	1283.325 mAh
Nominal voltage	3.7V
Charge cut-off voltage	4.2V (100% State of charge
Discharge cut-off voltage	(SOC))
Internal resistance of battery cell	3V (0% SOC)
Cathode and anode materials	54.175 mΩ
Cathode and anode thermal	Aluminium
conductivity	205 W/(mK)

Constant current (CC) charging is a technique for preventing overcurrent charge circumstances. It involves continually charging a rechargeable battery at a constant current. One way to avoid overcharging is by using constant voltage (CV) charging, which involves keeping the charging voltage constant. After a strong starting current, the charging current drops down over time. The battery management system controls the electrical battery pack to an alternating current power supply. The voltage and current are calibrated with the standard calibrator, with uncertainties of ±0.5V and ±0.05A, respectively. The C-rate parameters describe the charging and discharging rates. A C-rate of 1 means a fully charged 1 Ah battery (1 A in an hour), a 0.5 C-rate provides 0.5 A over two hours, or a C-rate of 2, 2 A for 30 min.

Table 2. Uncertainty and accuracy of the instruments.

Instruments	Accuracy	Uncertainty
Voltage supplied by power source, voltage	0.20%	±0.50
Current supplied by power source, ampere	0.20%	±0.50
Digital weight scale, gram	0.01%	±0.01
Thermocouple type T, Data logger, °C	0.10%	±0.10

3. Mathematical modeling

3.1 The main equations

Figure 5 shows the computational domains with two different coolant flow directions. Two different mini-channel fin heat inks with varying fin configurations have been considered, as shown in Fig. 6. Mathematical simulations are run with coolant passing through the aluminum jacket with a 3D Eulerian flow model with the equations[73,74] assuming a homogenous mixture, constant flow, no phase change, and no viscous dissipation.

Continuity equations:[73]

$$\nabla\left(\rho_p \phi_p V_p\right) = 0 \tag{1}$$

$$\nabla\left(\rho_l \phi_l V_l\right) = 0 \tag{2}$$

where ρ_p and ρ_l are particles and liquid densities, respectively, V_p and V_l are particles and liquid velocity, respectively, ϕ_p and ϕ_l are particles and liquid concentrations, respectively.

Momentum equations:[73]

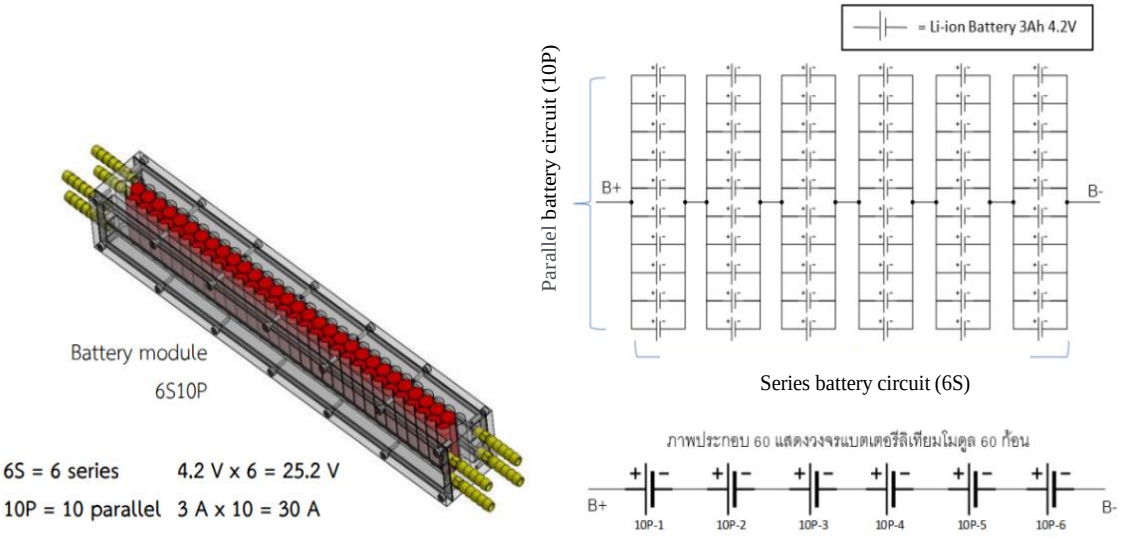

Fig. 4 Details of the battery cell connection used in the present study.

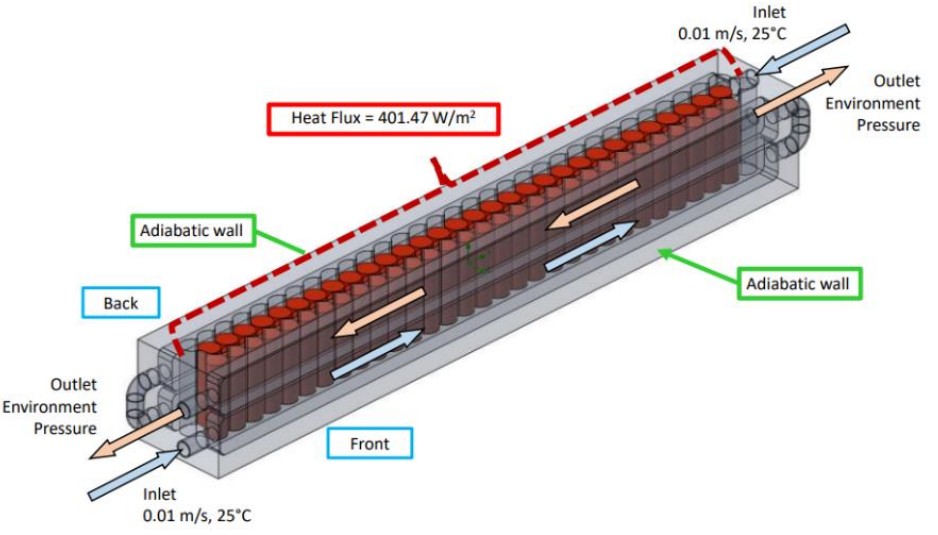

Fig. 5 Details of the computational domain.

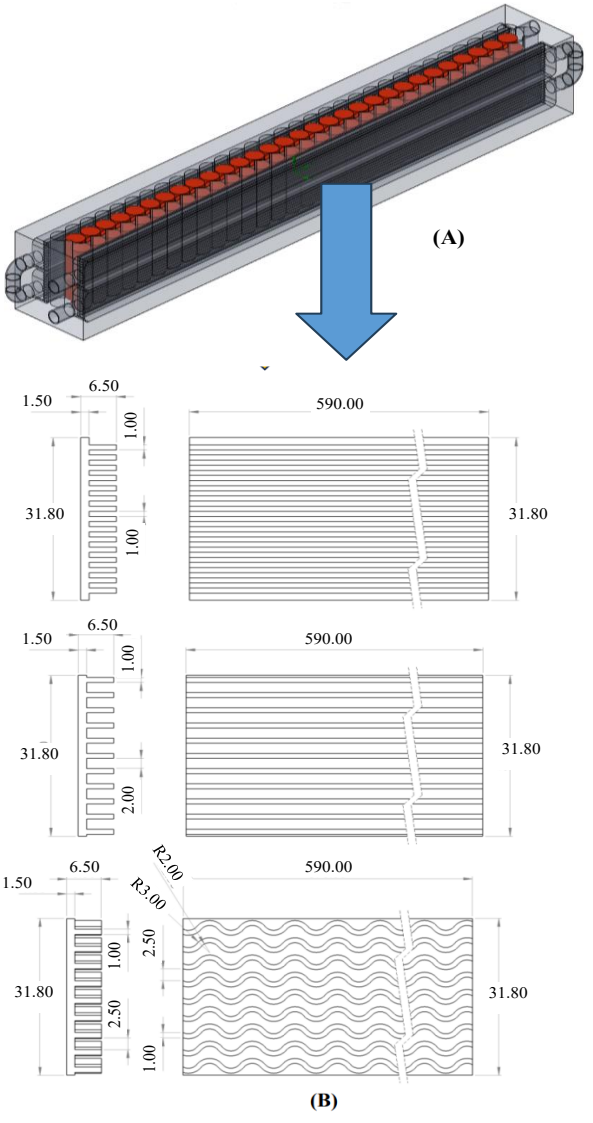

Fig. 6 Details of (A) the mini-fin heat sinks embedded at the flow channel and (B) mini-channel heat sink unit details.

$$\nabla(\rho_p\phi_p V_p V_p) = \phi_p\nabla P + \nabla\left(\phi_p\mu_p(\nabla V_p + \nabla V_p T)\right) - F_d + F_{Vm} + F_{cd} \quad (3)$$

$$\nabla(\rho_l\phi_l V_l V_l) = \phi_l\nabla P + \nabla\left(\phi_l\mu_l(\nabla V_l + \nabla V_l T)\right) + F_d + F_{Vm} \quad (4)$$

where μ_p and ρ_μ are particles and liquid viscosities, respectively, ∇P is pressure drop.

From [73], we may derive the drag force between nanoparticles in suspension and water, as seen in Eq. (5).

$$F_d = -\beta(V_l - V_p) \quad (5)$$

$$\beta = C_d\frac{3(1-\phi_l)\phi_l}{4d_p}(V_l - V_p)\phi_l^{-265} \quad (6)$$

$$C_d = \begin{cases}\frac{24}{Re_p}\left(1 + 0.15\,Re_p^{0.687}\right), & Re_p \langle 1000 \\ 0.44\,, & Re_p \rangle 1000\end{cases} \quad (7)$$

$$Re_p = \frac{\phi_l|V_l - V_p|d_p}{\nu_l} \quad (8)$$

where $\mathrm{Re_p}$ is the particle Reynolds number, ν_l is liquid viscosity and d_p is particle diameter.

Equation (9), following,[73] shows that the virtual mass force is proportional to the relative acceleration.

$$F_{Vm} = 0.5\phi_p\rho_l\frac{D(V_l - V_p)}{Dt} \quad (9)$$

According to Eq. (10), the relation establishes the contact force and modulus among the particles.[73]

$$F_{cd} = \phi_l\vec{\nabla}\phi_l(exp(-600[\phi_l - 0.376])) \quad (10)$$

Energy equations:[73]

Considering both phases, it is written as in Eq. (11) and Eq. (12).

$$\nabla(\rho_l\phi_l C_{p,l}T_l V_l) = \nabla(\phi_l k_l\nabla T_l) - h_v(T_l - T_p) \quad (11)$$

$$\nabla\left(\rho_p \phi_p C_{p,p} T_p V_p\right) = \nabla\left(\phi_p k_p \nabla T_p\right) - h_v\left(T_l - T_p\right) \quad (12)$$

where $C_{p,l}$ and $C_{p,p}$ are specific heat of liquid and liquid, respectively, k_l and k_p are thermal conductivity of liquid and particle, respectively, T_l and T_p are liquid and particle temperatures, respectively.

Here is the mono-dispersed particle (hv) as indicated in Eq. (13):

$$h_v = \frac{6(1-\phi_l)}{d_p}\left(2 + 1.1\, Re_p^{0.6}\, Pr^{\frac{1}{3}}\right)\frac{k_l}{d_p} \quad (13)$$

The effective thermal conductivities of liquid and particles (k_l, k_p) are obtained from [73], as shown in Eq. (14):

$$k_p = \frac{k_{bp}}{\phi_p},\ k_l = \frac{k_{bl}}{\phi_l}, A = \frac{k_p}{k_l} \quad (14)$$

$$k_{bp} = \left(\sqrt{(1-\phi_l)}\right)(\omega A + [0.9927]\Gamma)k_l \quad (15)$$

$$k_{bl} = \left(1 - \sqrt{(1-\phi_l)}\right)k_l \quad (16)$$

$$\Gamma = \frac{2A}{(A-B)}\left\{\frac{AB(A-1)}{(A-B)^2}\right\} ln\left(\frac{A}{B}\right) - \frac{(AB-A)}{(A-B)} - \frac{B+1}{2} \quad (17)$$

$$A = \frac{k_p}{k_l},\quad B = 1.25\left(\frac{1}{\phi_l} - 1\right)^{\frac{10}{9}} \quad (18)$$

Table 3. Thermophysical properties of water, Fe_3O_4 (25 °C).

Properties	Fe_3O_4
Density, ρ (kg/m^3)	5180
Thermal conductivity, k (W/m°C)	80.4
Viscosity, μ (mPa S)	-
Specific heat, C_p (J/kg.K)	670
Purity, (%)	>99.9
Average diameter, (nm)	23

3.2 Boundary conditions

The fluid flow channel was designed with two layers of different coolant flow directions to better model battery conditions. The channel's outside surfaces and the battery's top and base were insulated to prevent heat losses. Furthermore, to guarantee effective heat transfer throughout the system, the walls between the coolant and the cell surface were linked, with identical intake velocities enforced as boundary conditions and the cooling fluids selected to mimic those utilized in the packs closely. These boundary requirements were crucial in attaining precise results while keeping the battery safe and efficient. Finally, combining the relevant parts, including insulation and boundary conditions, enables precise and reliable modeling of the pack. Both phases flow into the cooling system with the same velocity, and coolant properties are calculated using postulated correlations based on base fluid and nanoparticle properties (Table 3).[75-78] The boundary conditions are presented as:

- Inlet: $T = T_{in}, V = V_{in}$
- Outlet: $P_{out} = o$
- Battery cell wall: $q = q_{in}$

-The cell battery and the aluminum interface:

$$-k_{ba}\frac{\partial T}{\partial n} = -k_{al}\frac{\partial T}{\partial n}$$

- The heat sink unit and the coolant interface:

$$-k_{al}\frac{\partial T}{\partial n} = h_c(T_{al} - T_{coo})$$

where $\frac{\partial T}{\partial n}$ is the temperature gradient in the normal direction.

3.3 Computational methodology

The numerical analysis was performed with four models, as shown in Fig. 7. This study used the multi-scale multi-domain (MSMD) technique in FLUENT Software to model a battery pack's electrical and thermal characteristics. ANSYS program is widely utilized in various engineering applications. After generating the model and mesh, the ANSYS Fluent program solves the problems with the required boundary conditions using the SIMPLE technique, which combines the pressure and velocity components. It aids in the resolution of complex fluid flow problems by simplifying the pressure-velocity calculations. Setting adequate convergence conditions for the simulation is crucial for producing accurate and reliable findings. For this study, the convergence criterion was set to 10^{-6} to ensure the simulation values converged within limits. Incompressibility and Newtonianity are features of the nanofluid. The steady state of the flow indicates that fluid properties do not fluctuate over time. The flow is in the laminar range, and the channel walls are smooth. 18 CPU cores and 96 GB of Random-Access Memory (RAM) are used to build a computationally intensive personal computer.

3.4 Grid independent study

The essential step in the process is the mesh independence test procedure, which ensures the reliability and accuracy of the results. It is possible to determine the point at which further refining of the mesh grid no longer significantly improves the accuracy of the findings using three different mesh numbers. The grid configuration is shown in Fig. 8. This simplifies simulation execution by choosing the lowest possible mesh size, saving computing resources and shortening the entire process time. Table 4 shows various element sizes with the most significant temperature fluctuation (Model II). A constant coolant velocity was applied to the cooling jacket of 0.01 m/s, and 25 inlet temperatures entered the cooling channel. An average pack temperature was compared to see how different grid numbers affected the predicted results. The

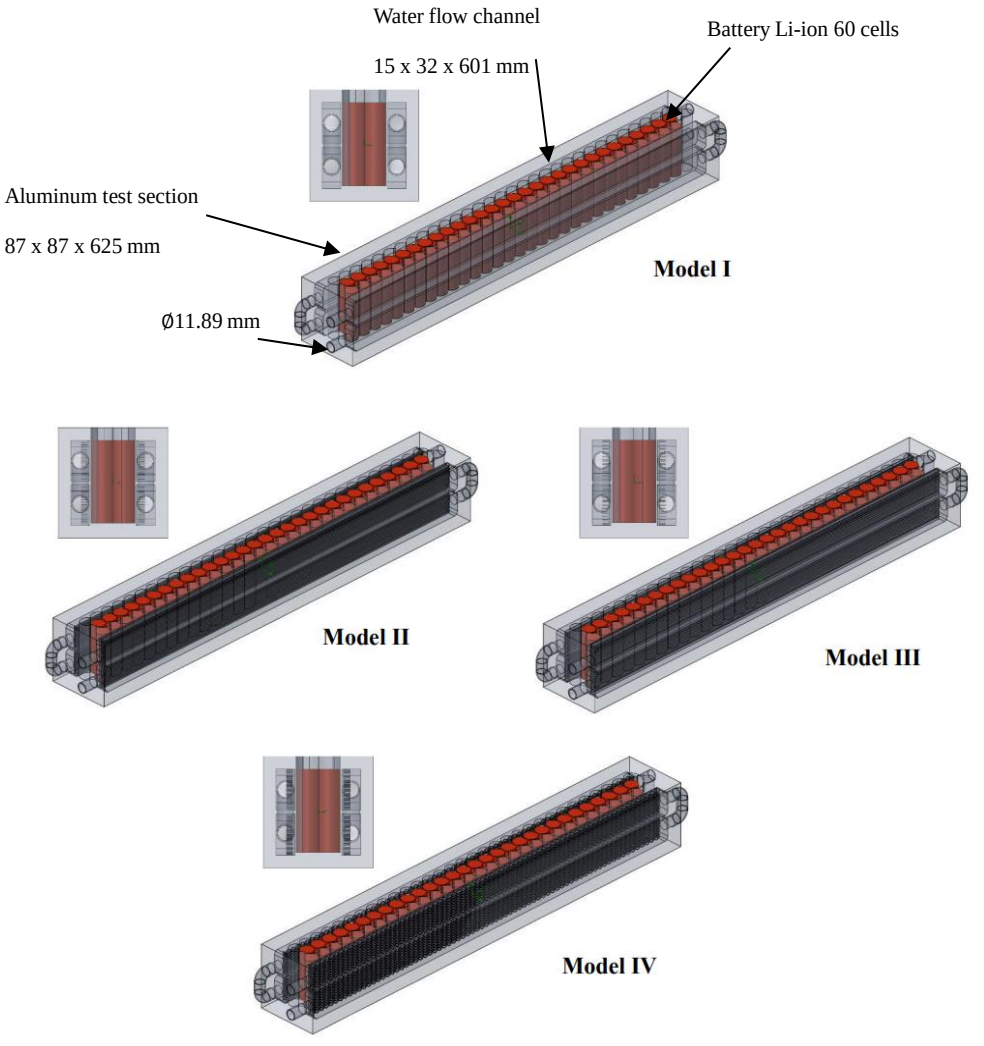

Fig. 7 Problem models used in the numerical analysis for model I (without the heat sink unit), model II (with the straight fin heat sink (fs=1 mm)), model III (with the straight fin heat sink (fs=2 mm)), and model IV (with the arced fin heat sink).

Table 4. Grid-independent test.

Grids	Average battery temperature at the front zone(ºC)	% error	Average battery temperature at the back zone (ºC)	% error
3,800,000	30.13		30.23	
7,477,000	29.38	2.52	29.28	3.19
7,725,000	29.37	0.03	29.25	0.10

mesh independence process discovered a minor variation in temperature readings obtained with various grid numbers.

Consequently, the grid numbers did not significantly affect the predicted results, indicating that the process was stable and valid. The remaining simulations were run using grid numbers of 7,477,000, providing a good mix of accuracy and computing efficiency while accurately capturing the battery fluid movement and heat transfer. The temperature variation has a substantial positive relationship, with the most notable difference between the coarse and medium meshes, where the gap is significantly less than the allowable error level of 1% for computational fluid dynamics (CFD) solutions, showing that the mesh resolution is adequate.

3.5 Verification of the numerical study

To lessen the impact of outside air temperature, an experiment was carried out at a control room temperature of 25 °C. Due to the power supply unit limitations, experimental procedures were carried out at a low C-rate. Based on the system pre-test, the energy storage battery took 9 minutes to charge and 5 minutes to discharge. The pack operating temperature is less than 40 °C to ensure extended life, stability, and safety.[79] The temperature fluctuations throughout the charging and discharging operations are consistent with previously

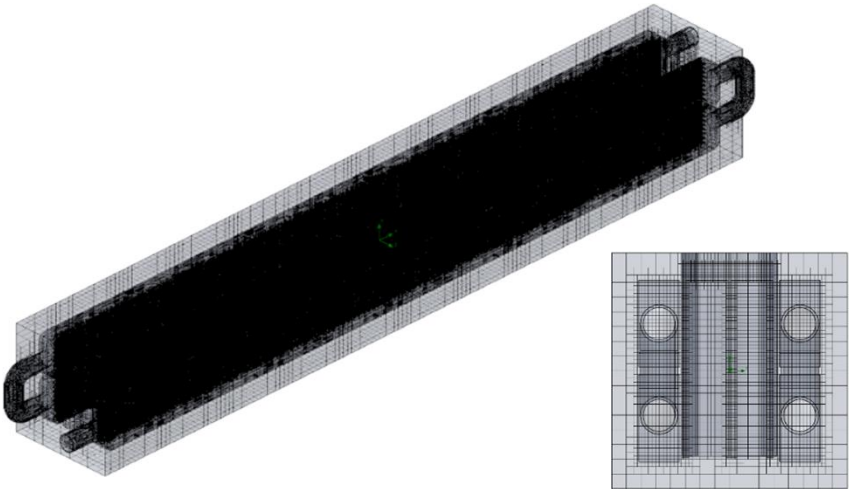

Fig. 8 Grid characteristics used in the present numerical analysis.

Table 5. Comparison between the measured data and the predicted results (Model I).

Average battery temperature	Experimental results	Predicted results	%error
Upper zone (FA)	31.6	29.66	6.33
Lower zone (FA)	30.11	29.23	2.97
Upper zone (BA)	32.86	29.76	9.90
Lower zone (BA)	30.87	29.93	3.09

published work, which shows modest drops and slight rises for the charging and discharging processes.[80] To confirm the expected outcomes, the numerical research findings must be validated. Cooling models were created for the experiment, and the experimental set was set to validate the predicted outcomes. The average battery pack temperatures of the higher and lower zones (for further information, see [59]) were chosen to validate the projected findings. Table 5 shows that model I has the highest inaccuracy in the front upper flow channel (6.33%) and the back upper flow channel (9.90%).

4. Results and discussion

Figure 9 shows the variation temperature of the battery cells for different models. To reduce the highest temperature and temperature gradient, divide the flow into two streams with opposing flow characteristics, as shown in Fig. 5. Firstly, the mainstream enters the pack from the front lower flow channel. It exits via the front upper flow channel. The second, the mainstream enters at the other end (back upper flow channel) and exits at the back lower flow channel. In the numerical analysis, four different models (Fig. 7) have been considered as follows;

Model I: the liquid flow channel without the heat sink unit.

Model II: the liquid flow channel embedded with the straight fin heat sink (fs=1 mm).

Model III: the liquid flow channel embedded with the straight fin heat sink (fs=2 mm).

Model IV: Model II: the liquid flow channel embedded with the arced fin heat sink.

Typically, the heat generated by the cell during charging and discharging consists of reaction heat released by chemical reactions, polarization heat generated by the equilibrium of electrode potential shift, Joule heat generated by the battery's internal resistance, and side reaction heat released by the side reaction between the electrolyte and the electrodes. As operating time grows without cooling, the overall pack temperature rises due to accumulated heat, with the maximum temperature occurring in the inner zone. The generated heat from the pack is transferred to the exterior surface, then to the jacket of the flow channel via conduction, and finally cooled by the coolant (Model I). Therefore, the cell temperature increases downstream, then the maximum is at the middle zone of the pack, and then it decreases at another end. The coolant's heat removal ability decreases as its temperature increases. The heat transfer surface area and the thermophysical qualities of the coolant restrict the heat transmission from the battery cell to the jacket via conduction and subsequently to the coolant via convection. The temperature of 47 cells is close to 30 ºC, which may rise in the worst-case scenario, as illustrated in Model I.

The BTMS design is crucial to pack longevity, performance, and safety issues. A battery pack functions at temperatures range of 15 °C - 35 °C. To reduce unpleasant effects, the optimal temperature gradient is smaller than five

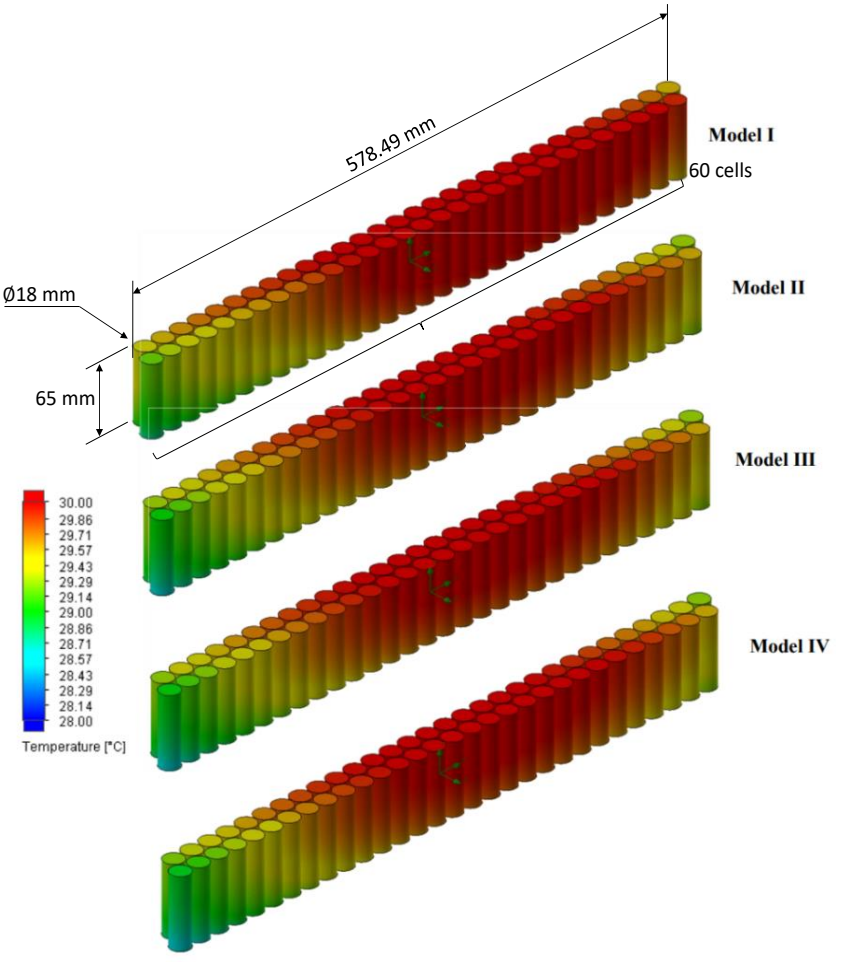

Fig. 9 Battery temperature distribution of different models.

degrees.[65] If the battery temperature exceeds this threshold, the anodic coating decomposes. Under high operating conditions, the electrolyte evaporates, and the pressure inside the cell builds, possibly causing the battery to fail mechanically. The heat accelerates the process by increasing the temperature and initiating a series of exothermal chemical reactions inside each cell. The uncontrolled increase in temperature and pressure within the battery causes the electrolyte to degenerate, leak, burn, and explode. As shown in Model I, almost all cells stay at high temperatures due to the limitations of heat transfer from the flow channel jacket to the coolant. As a result, the thermophysical properties of the coolant and heat transfer surface area were chosen to enhance the heat removal ability. In addition, the flow disturbance of coolant passing the arced-fin heat sink unit is considered, in which the embedded heat sink unit has a higher heat transfer surface area and a higher turbulent flow disturbance of coolant. Therefore, heat transfer ability depends on the heat transfer surface area and turbulent disturbance, in which Models II-IV have more heat transfer surface than Model I.

The battery cell temperatures without a mini-heat sink unit case are higher than those with a mini-heat sink unit, as shown in Fig. 10. Due to higher heat transfer surface area, lower fin space (Model I) gives the battery cell temperature lower than higher ones (Models III, IV). In addition, the fin configuration significantly affects the flow pattern and disturbance near the surface. The temperature distribution for the arced fin is better than that of the straight fin unit for the same fin space value. However, for the present study, the Model IV with higher fin space gives the battery cell temperature more than the Model III. The maximum temperatures with three different heat sink units are lower than those without heat sink units, as shown in Fig. 11, in which the maximum temperatures are 30.91 °C (Model I), 30.10 °C (Model II), 30.11 °C (Model III), and 30.12 °C (Model IV). The maximum temperature location occurs at the central area and upper zone. In addition, the number of cell batteries has a temperature near 30 °C, less than 47 cells, as shown in Figs. 11 and 12. This is because the embedded mini-fin heat sink unit significantly affects the conduction heat transfer in the flow direction of coolant.

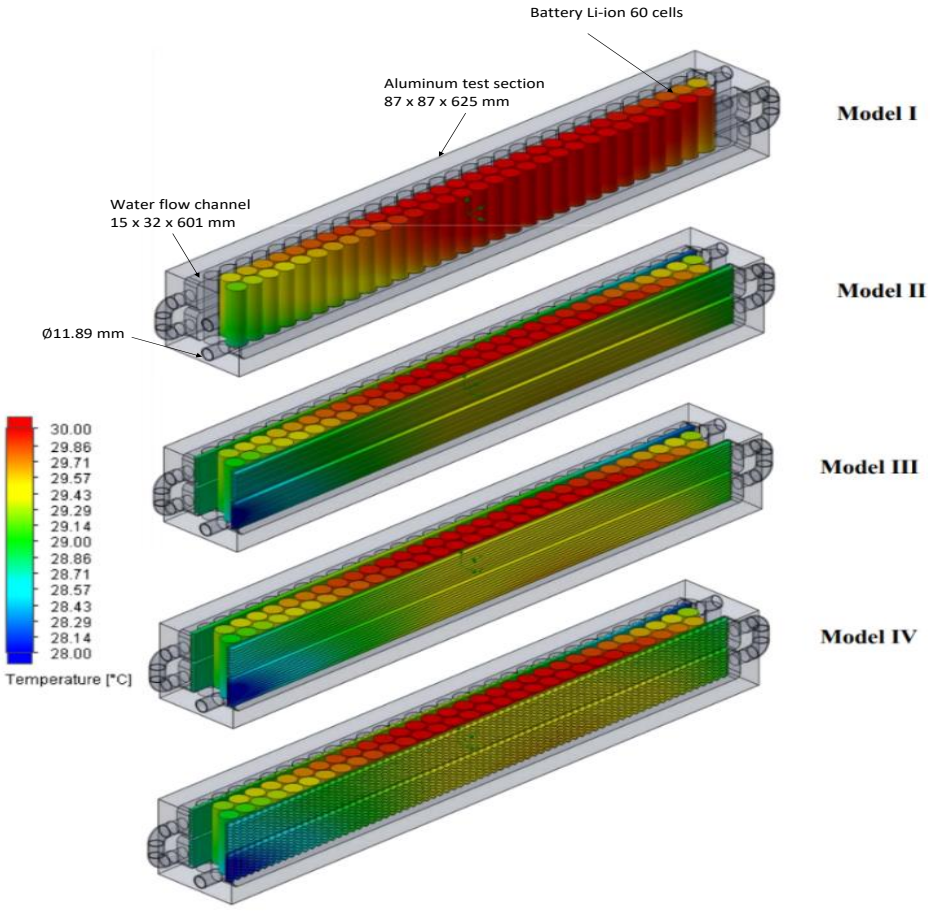

Fig. 10 Temperature distributions of the battery cell and mini-channel heat sink units

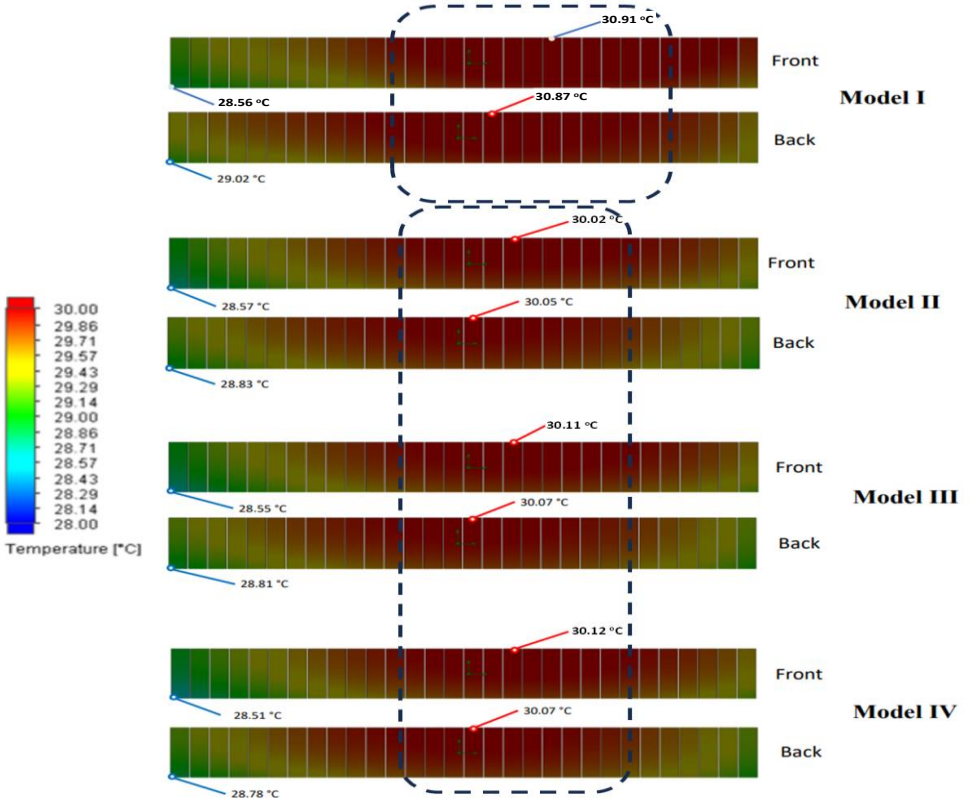

Fig. 11 Maximum and minimum temperature of the battery pack from different cooling models.

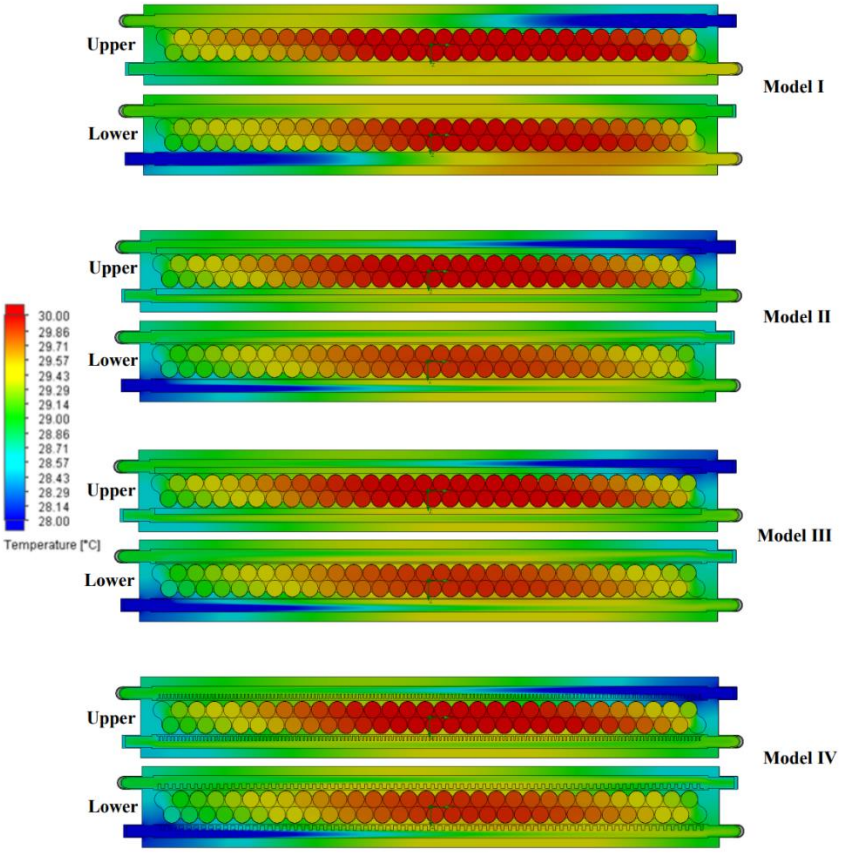

Fig. 12 Coolant temperature distribution from different cooling models.

5. Conclusions

Thermal runaway may occur, causing a domino effect until each cell in the battery deteriorates, which can be caused by overcharging, short-circuiting, or exposure to external heat. The peak temperature and the temperature gradient are critical to battery life, performance, and safety concerns. A battery pack performs best at temperatures ranging from 15 °C to 35 °C. Models I and II show the highest and lowest temperatures, respectively. Models I, II, III, and IV have temperature gradients of 2.35 °C, 1.48 °C, 1.56 °C, and 1.61 °C, respectively. The development of the BTMS has significant implications based on these results. Engineers can optimize the cooling thermal process by incorporating different heat transfer enhancement techniques to enhance thermal cooling efficiency while maintaining safety and stability.

Acknowledgments

Srinakharinwirot University provided some funding for this study, which the authors gratefully acknowledge.

Conflict of Interest

There is no conflict of interest.

Supporting Information

Not applicable.

Nomenclatures

A	defined in Eq. (18), [-]
BTMS	battery thermal management system
C_d	defined in Eq. (7), [-]
EV	electric vehicle
fs	fin spacing, [m]
h	heat transfer coefficient, [kW m^{-2} ^{o}C^{-1}]
h_p	fluid-particle heat transfer coefficient, [kW m^{-2} ^{o}C^{-1}]
k	thermal conductivity, [kW m^{-1} ^{o}C^{-1}]
k_{bl}	defined in Eq. (16), [kW m^{-1} ^{o}C^{-1}]
LIB	Lithium battery
P	pressure, [kPa]
PCM	phase change material
SOC	State of charge
V	velocity, [m s^{-1}]
B	defined in Eq. (18), [-]

BMS	battery management system
C_p	specific heat, [kJ kg^{-1} ^{o}C^{-1}]
F	force, [N]
h_v	volumetric interphase heat transfer coefficient, [kW m^{-3} ^{o}C^{-1}]
HEV	Hybrid electric vehicle
I	current, [ampere]
k_{bp}	defined in Eq. (15), [kW m^{-1} ^{o}C^{-1}]
Li-ion	Lithium-ion
OCV	Open circuit voltage
Q	generated heat. [kW]
Re	Reynolds number based on inlet diameter
T	temperature, [^{o}C]

Greek symbols

ϕ	nanofluid concentration, [%]
β	defined in Eq. (6), [kg m^{-3}s^{-1}]
ρ	density, [kg m^{-3}]
μ	viscosity, [kg m^{-1}s^{-1}]

Subscripts

al	aluminium
c	convective
coo	coolant
in	inlet
p	particles
ba	cell battery
cd	drag coefficient
d	drag force
l	liquid
Vm	virtual mass

References

[1] A. K. Thakur, R. Prabakaran, M. R. Elkadeem, S. W. Sharshir, M. Arıcı, C. Wang, W. Zhao, J.-Y. Hwang, R. Saidur, A state of art review and future viewpoint on advance cooling techniques for Lithium–ion battery system of electric vehicles, *Journal of Energy Storage*, 2020, **32**, 101771, doi: 10.1016/j.est.2020.101771.

[2] L. H. Saw, Y. Ye, A. A. O. Tay, Integration issues of lithium-ion battery into electric vehicles battery pack, *Journal of Cleaner Production*, 2016, **113**, 1032-1045, doi: 10.1016/j.jclepro.2015.11.011.

[3] A. A. Pesaran, Battery thermal models for hybrid vehicle simulations, *Journal of Power Sources*, 2002, **110**, 377-382, doi: 10.1016/s0378-7753(02)00200-8.

[4] Y. Xu, H. Zhang, X. Xu, X. Wang, Numerical analysis and surrogate model optimization of air-cooled battery modules using double-layer heat spreading plates, *International Journal of Heat and Mass Transfer*, 2021, **176**, 121380, doi: 10.1016/j.ijheatmasstransfer.2021.121380.

[5] G. Zhao, X. Wang, M. Negnevitsky, H. Zhang, C. Li, Performance improvement of a novel trapezoid air-cooling battery thermal management system for electric vehicles, *Sustainability*, 2022, **14**, 4975, doi: 10.3390/su14094975.

[6] G. Zhao, X. Wang, M. Negnevitsky, A study of variable cell spacings to the heat transfer efficiency of air-cooling battery thermal management system, *Applied Sciences*, 2021, **11**, 11155, doi: 10.3390/app112311155.

[7] D. Chen, J. Jiang, G.-H. Kim, C. Yang, A. Pesaran, Comparison of different cooling methods for lithium-ion battery cells, *Applied Thermal Engineering*, 2016, **94**, 846-854, doi: 10.1016/j.applthermaleng.2015.10.015.

[8] F. Chen, R. Huang, C. Wang, X. Yu, H. Liu, Q. Wu, K. Qian, R. Bhagat, Air and PCM cooling for battery thermal management considering battery cycle life, *Applied Thermal Engineering*, 2020, **173**, 115154, doi: 10.1016/j.applthermaleng.2020.115154.

[9] X. Lin, X. Zhang, J. Ji, L. Liu, Y. Wu, M. Yang, D. Lu, H. Zheng, Development of flexible form-stable phase change material with enhanced electrical resistance for thermal management, *Journal of Cleaner Production*, 2021, **311**, 127517, doi: 10.1016/j.jclepro.2021.127517.

[10] S. Panchal, I. Dincer, M. Agelin-Chaab, R. Fraser, M. Fowler, Thermal modeling and validation of temperature distributions in a prismatic lithium-ion battery at different discharge rates and varying boundary conditions, *Applied Thermal Engineering*, 2016, **96**, 190-199, doi: 10.1016/j.applthermaleng.2015.11.019.

[11] Z. J. Tang, Q. Z. Zhu, J. W. Lu, M. Y. Wu, Study on various types of cooling techniques applied to power battery thermal management systems, *Advanced Materials Research*, 2012, **608**, 1571-1576, doi: 10.4028/www.scientific.net/amr.608-609.1571.

[12] K. Chen, X. Li, Accurate determination of battery discharge characteristics–A comparison between two battery temperature control methods, *Journal of Power Sources*, 2014, **247**, 961-966, doi: 10.1016/j.jpowsour.2013.09.060.

[13] M.-S. Liu, M. C.-C. Lin, C. Y. Tsai, C.-C. Wang, Enhancement of thermal conductivity with Cu for nanofluids using chemical reduction method, *International Journal of Heat and Mass Transfer*, 2006, **49**, 3028-3033, doi: 10.1016/j.ijheatmasstransfer.2006.02.012.

[14] S. A. Angayarkanni, J. Philip, Effect of nanoparticles aggregation on thermal and electrical conductivities of nanofluids, *Journal of Nanofluids*, 2014, **3**, 17-25, doi: 10.1166/jon.2014.1083.

[15] Y. Deng, C. Feng, E. Jiaqiang, H. Zhu, J. Chen, M. Wen, H. Yin, Effects of different coolants and cooling strategies on the cooling performance of the power lithium ion battery system: a review, *Applied Thermal Engineering*, 2018, **142**, 10-29, doi: 10.1016/j.applthermaleng.2018.06.043.

[16] H.-L. Liu, X.-K. An, C.-S. Wang, Heat transfer performance of T-Y type micro-channel heat sink with liquid GaInSn coolant, *International Journal of Thermal Sciences*, 2017, **120**, 203-219, doi: 10.1016/j.ijthermalsci.2017.06.008.

[17] J. Zhao, Z. Rao, Y. Li, Thermal performance of mini-channel liquid cooled cylinder-based battery thermal management for cylindrical lithium-ion power battery, *Energy Conversion and Management*, 2015, **103**, 157-165, doi: 10.1016/j.enconman.2015.06.056.

[18] C. Lan, J. Xu, Y. Qiao, Y. Ma, Thermal management for

high power lithium-ion battery by minichannel aluminum tubes, *Applied Thermal Engineering*, 2016, **101**, 284-292, doi: 10.1016/j.applthermaleng.2016.02.070.
[19] E. Jiaqiang, D. Han, A. Qiu, H. Zhu, Y. Deng, J. Chen, X. Zhao, W. Zuo, H. Wang, J. Chen, Q. Peng, Orthogonal experimental design of liquid-cooling structure on the cooling effect of a liquid-cooled battery thermal management system, *Applied Thermal Engineering*, 2018, **132**, 508-520, doi: 10.1016/j.applthermaleng.2017.12.115.
[20] W. Cao, C. Zhao, Y. Wang, T. Dong, F. Jiang, Thermal modeling of full-size-scale cylindrical battery pack cooled by channeled liquid flow, *International Journal of Heat and Mass Transfer*, 2019, **138**, 1178-1187, doi: 10.1016/j.ijheatmasstransfer.2019.04.137.
[21] L. Sheng, L. Su, H. Zhang, K. Li, Y. Fang, W. Ye, Y. Fang, Numerical investigation on a lithium ion battery thermal management utilizing a serpentine-channel liquid cooling plate exchanger, *International Journal of Heat and Mass Transfer*, 2019, **141**, 658-668, doi: 10.1016/j.ijheatmasstransfer.2019.07.033.
[22] L. Xie, Y. Huang, H. Lai, Coupled prediction model of liquid-cooling based thermal management system for cylindrical lithium-ion module, *Applied Thermal Engineering*, 2020, **178**, 115599, doi: 10.1016/j.applthermaleng.2020.115599.
[23] W. Li, A. Garg, M. Xiao, L. Gao, Optimization for liquid cooling cylindrical battery thermal management system based on Gaussian process model, *Journal of Thermal Science and Engineering Applications*, 2021, **13**, 021015, doi: 10.1115/1.4047526.
[24] B. Li, Z. Mao, B. Song, C. Lu, W. Tian, B. Zhang, Study on battery thermal management of autonomous underwater vehicle by bionic wave channels with liquid cooling, *International Journal of Energy Research*, 2021, **45**, 13269-13283, doi: 10.1002/er.6652.
[25] S. C. Chen, C. C. Wan, Y. Y. Wang, Thermal analysis of lithium-ion batteries, *Journal of Power Sources*, 2005, **140**, 111-124, doi: 10.1016/j.jpowsour.2004.05.064.
[26] B. Coleman, J. Ostanek, J. Heinzel, Reducing cell-to-cell spacing for large-format lithium ion battery modules with aluminum or PCM heat sinks under failure conditions, *Applied Energy*, 2016, **180**, 14-26, doi: 10.1016/j.apenergy.2016.07.094.
[27] T. Zhang, Q. Gao, G. Wang, Y. Gu, Y. Wang, W. Bao, D. Zhang, Investigation on the promotion of temperature uniformity for the designed battery pack with liquid flow in cooling process, *Applied Thermal Engineering*, 2017, **116**, 655-662, doi: 10.1016/j.applthermaleng.2017.01.069.
[28] S. Zhang, R. Zhao, J. Liu, J. Gu, Investigation on a hydrogel based passive thermal management system for lithium ion batteries, *Energy*, 2014, **68**, 854-861, doi: 10.1016/j.energy.2014.03.012.
[29] Y. Xu, X. Li, X. Liu, Y. Wang, X. Wu, D. Zhou, Experiment investigation on a novel composite silica gel plate coupled with liquid-cooling system for square battery thermal management, *Applied Thermal Engineering*, 2021, **184**, 116217, doi: 10.1016/j.applthermaleng.2020.116217.
[30] Z. Rao, Z. Qian, Y. Kuang, Y. Li, Thermal performance of liquid cooling based thermal management system for cylindrical lithium-ion battery module with variable contact surface, *Applied Thermal Engineering*, 2017, **123**, 1514-1522, doi: 10.1016/j.applthermaleng.2017.06.059.
[31] Z. Tang, S. Wang, Z. Liu, J. Cheng, Numerical analysis of temperature uniformity of a liquid cooling battery module composed of heat-conducting blocks with gradient contact surface angles, *Applied Thermal Engineering*, 2020, **178**, 115509, doi: 10.1016/j.applthermaleng.2020.115509.
[32] C. Li, Y. Li, S. Srinivaas, J. Zhang, S. Qu, W. Li, Mini-channel liquid cooling system for improving heat transfer capacity and thermal uniformity in battery packs for electric vehicles, *Journal of Electrochemical Energy Conversion and Storage*, 2021, **18**, 030905, doi: 10.1115/1.4050723.
[33] A. Jarrett, I. Y. Kim, Design optimization of electric vehicle battery cooling plates for thermal performance, *Journal of Power Sources*, 2011, **196**, 10359-10368, doi: 10.1016/j.jpowsour.2011.06.090.
[34] A. Jarrett, I. Y. Kim, Influence of operating conditions on the optimum design of electric vehicle battery cooling plates, *Journal of Power Sources*, 2014, **245**, 644-655, doi: 10.1016/j.jpowsour.2013.06.114.
[35] J. Smith, M. Hinterberger, C. Schneider, J. Koehler, Energy savings and increased electric vehicle range through improved battery thermal management, *Applied Thermal Engineering*, 2016, **101**, 647-656, doi: 10.1016/j.applthermaleng.2015.12.034.
[36] L. W. Jin, P. S. Lee, X. X. Kong, Y. Fan, S. K. Chou, Ultra-thin minichannel LCP for EV battery thermal management, *Applied Energy*, 2014, **113**, 1786-1794, doi: 10.1016/j.apenergy.2013.07.013.
[37] A. De Vita, A. Maheshwari, M. Destro, M. Santarelli, M. Carello, Transient thermal analysis of a lithium-ion battery pack comparing different cooling solutions for automotive applications, *Applied Energy*, 2017, **206**, 101-112, doi: 10.1016/j.apenergy.2017.08.184.
[38] W. Li, L. Li, W. Cui, M. Guo, Experimental investigation on the thermal performance of vapor chamber in a compound liquid cooling system, *International Journal of Heat and Mass Transfer*, 2021, **170**, 121026, doi: 10.1016/j.ijheatmasstransfer.2021.121026.
[39] W. Tong, K. Somasundaram, E. Birgersson, A. S. Mujumdar, C. Yap, Numerical investigation of water cooling for a lithium-ion bipolar battery pack, *International Journal of Thermal Sciences*, 2015, **94**, 259-269, doi: 10.1016/j.ijthermalsci.2015.03.005.
[40] Y. Huo, Z. Rao, X. Liu, J. Zhao, Investigation of power battery thermal management by using mini-channel cold plate, *Energy Conversion and Management*, 2015, **89**, 387-395, doi: 10.1016/j.enconman.2014.10.015.
[41] Z. Qian, Y. Li, Z. Rao, Thermal performance of lithium-ion battery thermal management system by using mini-channel cooling, *Energy Conversion and Management*, 2016, **126**, 622-631, doi: 10.1016/j.enconman.2016.08.063.
[42] C. Wang, G. Zhang, X. Li, J. Huang, Z. Wang, Y. Lv, L. Meng,

W. Situ, M. Rao, Experimental examination of large capacity liFePO$_4$ battery pack at high temperature and rapid discharge using novel liquid cooling strategy, *International Journal of Energy Research*, 2018, **42**, 1172-1182, doi: 10.1002/er.3916.
[43] C. Wang, G. Zhang, L. Meng, X. Li, W. Situ, Y. Lv, M. Rao, Liquid cooling based on thermal silica plate for battery thermal management system, *International Journal of Energy Research*, 2017, **41**, 2468-2479, doi: 10.1002/er.3801.
[44] M. S. Patil, J.-H. Seo, S. Panchal, M.-Y. Lee, Numerical study on sensitivity analysis of factors influencing liquid cooling with double cold-plate for lithium-ion pouch cell, *International Journal of Energy Research*, 2021, **45**, 2533-2559, doi: 10.1002/er.5946.
[45] A. Karthik, P. Kalita, A. Garg, L. Gao, S. Chen, X. Peng, A Novel MOGA approach for power saving strategy and optimization of maximum temperature and maximum pressure for liquid cooling type battery thermal management system, *International Journal of Green Energy*, 2021, **18**, 80-89, doi: 10.1080/15435075.2020.1831507.
[46] S. Chen, N. Bao, A. Garg, X. Peng, L. Gao, A fast charging–cooling coupled scheduling method for a liquid cooling-based thermal management system for lithium-ion batteries, *Engineering*, 2021, **7**, 1165-1176, doi: 10.1016/j.eng.2020.06.016.
[47] A. Garg, C. Liu, A. K. Jishnu, L. Gao, M. L. Le Phung, V. M. Tran, A Thompson sampling efficient multi-objective optimization algorithm (TSEMO) for lithium-ion battery liquid-cooled thermal management system: study of hydrodynamic, thermodynamic, and structural performance, *Journal of Electrochemical Energy Conversion and Storage*, 2021, **18**, 021009, doi: 10.1115/1.4048537.
[48] J. Wang, S. Lu, Y. Wang, Y. Ni, S. Zhang, Novel investigation strategy for mini-channel liquid-cooled battery thermal management system, *International Journal of Energy Research*, 2020, **44**, 1971-1985, doi: 10.1002/er.5049.
[49] R. W. Van Gils, D. Danilov, P. H. L. Notten, M. F. M. Speetjens, H. Nijmeijer, Battery thermal management by boiling heat-transfer, *Energy Conversion and Management*, 2014, **79**, 9-17, doi: 10.1016/j.enconman.2013.12.006.
[50] Y.-F. Wang, J.-T. Wu, Thermal performance predictions for an HFE-7000 direct flow boiling cooled battery thermal management system for electric vehicles, *Energy Conversion and Management*, 2020, **207**, 112569, doi: 10.1016/j.enconman.2020.112569.
[51] H. Hirano, T. Tajima, T. Hasegawa, T. Sekiguchi, M. Uchino, Boiling liquid battery cooling for electric vehicle, 2014 IEEE Conference and Expo Transportation Electrification Asia-Pacific (ITEC Asia-Pacific). Beijing, China. IEEE, 2014.
[52] Z. An, L. Jia, X. Li, Y. Ding, Experimental investigation on lithium-ion battery thermal management based on flow boiling in mini-channel, *Applied Thermal Engineering*, 2017, **117**, 534-543, doi: 10.1016/j.applthermaleng.2017.02.053.
[53] X. Tan, P. Lyu, Y. Fan, J. Rao, K. Ouyang, Numerical investigation of the direct liquid cooling of a fast-charging lithium-ion battery pack in hydrofluoroether, *Applied Thermal Engineering*, 2021, **196**, 117279, doi: 10.1016/j.applthermaleng.2021.117279.
[54] M. Al-Zareer, I. Dincer, M. A. Rosen, Electrochemical modeling and performance evaluation of a new ammonia-based battery thermal management system for electric and hybrid electric vehicles, *Electrochimica Acta*, 2017, **247**, 171-182, doi: 10.1016/j.electacta.2017.06.162.
[55] X.-H. Yang, S.-C. Tan, J. Liu, Thermal management of Li-ion battery with liquid metal, *Energy Conversion and Management*, 2016, **117**, 577-585, doi: 10.1016/j.enconman.2016.03.054.
[56] Z. Liu, H. Wang, C. Yang, J. Zhao, Simulation study of lithium-ion battery thermal management system based on a variable flow velocity method with liquid metal, *Applied Thermal Engineering*, 2020, **179**, 115578, doi: 10.1016/j.applthermaleng.2020.115578.
[57] H. Li, X. Xiao, Y. Wang, C. Lian, Q. Li, Z. Wang, Performance investigation of a battery thermal management system with microencapsulated phase change material suspension, *Applied Thermal Engineering*, 2020, **180**, 115795, doi: 10.1016/j.applthermaleng.2020.115795.
[58] S. Wiriyasart, C. Hommalee, S. Sirikasemsuk, R. Prurapark, P. Naphon, Thermal management system with nanofluids for electric vehicle battery cooling modules, *Case Studies in Thermal Engineering*, 2020, **18**, 100583, doi: 10.1016/j.csite.2020.100583.
[59] S. Sirikasemsuk, S. Wiriyasart, P. Naphon, N. Naphon, Thermal cooling characteristics of Li-ion battery pack with thermoelectric ferrofluid cooling module, *International Journal of Energy Research*, 2021, **45**, 8824-8836, doi: 10.1002/er.6417.
[60] S. Sirikasemsuk, S. Wiriyasart, R. Prurapark, N. Naphon, P. Naphon, Water/nanofluid pulsating flow in thermoelectric module for cooling electric vehicle battery systems, *International Journal of Heat and Technology*, 2021, **39**, 1618-1626, doi: 10.18280/ijht.390525.
[61] S. Sirikasemsuk, S. Wiriyasart, N. Naphon, P. Naphon, Flow direction effects on Li-ion cylindrical battery management cooling system with water/ferrofluid as coolants, *Frontiers in Heat Mass Transfer*, 2022, **19**, 1-11, doi: 10.5098/hmt.19.31.
[62] S. Sirikasemsuk, N. Naphon, S. Eiamsa-ard, P. Naphon, Analysis of nanofluid flow and heat transfer behavior of Li-ion battery modules, *International Journal of Heat and Mass Transfer*, 2023, **208**, 124058, doi: 10.1016/j.ijheatmasstransfer.2023.124058.
[63] S. Sirikasemsuk, P. Vengsungnle, S. Eiamsa-ard, P. Naphon, Thermal management of prismatic LiFePO$_4$ battery module with inversed-zigzag channeled ferrofluid flows, *Engineered Science*, 2023, **27**, 1017, doi: 10.30919/es1017.
[64] S. Sirikasemsuk, N. Naphon, P. Naphon, Investigation into thermal cooling with different ferrofluid flow arrangements for a lithium-ion battery pack, *Heat Transfer Engineering*, 2024, **45**, 1257-1273, doi: 10.1080/01457632.2023.2249733.
[65] M. Tousi, A. Sarchami, M. Kiani, M. Najafi, E. Houshfar, Numerical study of novel liquid-cooled thermal management system for cylindrical Li-ion battery packs under high discharge rate based on AgO nanofluid and copper sheath, *Journal of*

Energy Storage, 2021, **41**, 102910, doi: 10.1016/j.est.2021.102910.
[66] B. Mondal, C. F. Lopez, P. P. Mukherjee, Exploring the efficacy of nanofluids for lithium-ion battery thermal management, *International Journal of Heat and Mass Transfer*, 2017, **112**, 779-794, doi: 10.1016/j.ijheatmasstransfer.2017.04.130.
[67] P. Kritzer, H. Döring, B. Emermacher, Improved Safety for Automotive Lithium Batteries: an Innovative Approach to include an Emergency Cooling Element, *Advances in Chemical Engineering and Science*, 2014, **4**, 197-207, doi: 10.4236/aces.2014.42023.
[68] S. Chen, N. Bao, L. Gao, X. Peng, A. Garg, An experimental investigation of liquid cooling scheduling for a battery module, *International Journal of Energy Research*, 2020, **44**, 3020-3032, doi: 10.1002/er.5132.
[69] G. Chang, X. Cui, Y. Li, Y. Ji, Effects of reciprocating liquid flow battery thermal management system on thermal characteristics and uniformity of large lithium-ion battery pack, *International Journal of Energy Research*, 2020, **44**, 6383-6395, doi: 10.1002/er.5363.
[70] M.-K. Tran, A. DaCosta, A. Mevawalla, S. Panchal, M. Fowler, Comparative study of equivalent circuit models performance in four common lithium-ion batteries: LFP, NMC, LMO, NCA, *Batteries*, 2021, **7**, 51, doi: 10.3390/batteries7030051.
[71] J. Chen, P. Kollmeyer, S. Panchal, Y. Masoudi, O. Gross, A. Emadi, Experimental results of battery power capability measurement on cells with different state of health levels, 2024 IEEE Transportation Electrification Conference and Expo (ITEC). Chicago, IL, USA. IEEE, 2024.
[72] V. Talele, U. Moralı, H. Najafi Khaboshan, M. S. Patil, S. Panchal, R. Fraser, M. Fowler, Improving battery safety by utilizing composite phase change material to delay the occurrence of thermal runaway event, *International Communications in Heat and Mass Transfer*, 2024, **155**, 107527, doi: 10.1016/j.icheatmasstransfer.2024.107527.
[73] M. Akbari, N. Galanis, A. Behzadmehr, Comparative analysis of single and two-phase models for CFD studies of nanofluid heat transfer, *International Journal of Thermal Sciences*, 2011, **50**, 1343-1354, doi: 10.1016/j.ijthermalsci.2011.03.008.
[74] M. Kalteh, A. Abbassi, M. Saffar-Avval, A. Frijns, A. Darhuber, J. Harting, Experimental and numerical investigation of nanofluid forced convection inside a wide microchannel heat sink, *Applied Thermal Engineering*, 2012, **36**, 260-268, doi: 10.1016/j.applthermaleng.2011.10.023.
[75] B. C. Pak, Y. I. Cho, Hydrodynamic and heat transfer study of dispersed fluids with submicron metallic oxide particles, *Experimental Heat Transfer*, 1998, **11**, 151-170, doi: 10.1080/08916159808946559.
[76] Y. Xuan, W. Roetzel, Conceptions for heat transfer correlation of nanofluids, *International Journal of Heat and Mass Transfer*, 2000, **43**, 3701-3707, doi: 10.1016/s0017-9310(99)00369-5.
[77] D. A. Drew, S. L. Passman, Theory of multicomponent fluids, 1999.
[78] J. C. Maxwell, A Treatise on electricity and magnetism, 1881.
[79] A. Nazari, S. Farhad, Heat generation in lithium-ion batteries with different nominal capacities and chemistries, *Applied Thermal Engineering*, 2017, **125**, 1501-1517, doi: 10.1016/j.applthermaleng.2017.07.126.
[80] A. A. Pesaran, Battery thermal models for hybrid vehicle simulations, *Journal of Power Sources*, 2002, **110**, 377-382, doi: 10.1016/s0378-7753(02)00200-8.